Ouyang *et al. Microstructures* **2025**, *5*, 2025013
DOI: 10.20517/microstructures.2024.54

Microstructures

Research Article

Open Access

Investigation of the biocompatibility and osteogenic effects of magnesium-doped chloride-containing bioactive glasses

Zechi Ouyang[1], Piao Li[1], Xiaomei Ru[1], Linghao Liu[1], Priyen Shah[2], Ousheng Liu[1], Robert Hill[2], Xiaohui Chen[3], Xiaojing Chen[1,2]

[1]Hunan Key Laboratory of Oral Health Research and Academician Workstation for Oral-maxillofacial and Regenerative Medicine and Xiangya Stomatological Hospital and Xiangya School of Stomatology, Central South University, Changsha, 410008, Hunan, China.
[2] Institute of Dentistry, Dental Physical Sciences Unit, Barts and The London School of Medicine and Dentistry, Queen Mary University of London, E1 4NS, UK
[3]Division of Dentistry, School of Medical Sciences, The University of Manchester, Manchester, M13 9PL, UK.

Correspondence to: Prof. Xiaojing Chen, Xiangya School of Stomatology, Central South University, NO.64 Xiama Yuanling Xiang, Kaifu district, Changsha, 410008, China. E-mail: xiaojing.chen@csu.edu.cn

How to cite this article: Ouyang, Z.; Li, P.; Ru, X.; Liu, L.; Shah, P.; Liu, O.; Hill, R.; Chen, X.; Chen, X. Investigation of the biocompatibility and osteogenic effects of magnesium-doped chloride-containing bioactive glasses. *Microstructures* **2025**, *5*, 2025013. https://dx.doi.org/10.20517/microstructures.2024.54

Received: 30 Jun 2024 **First Decision:** 4 Sep 2024 **Revised:** 26 Nov 2024 **Accepted:** 13 Dec 2024 **Published:** 26 Jan 2025

Academic Editor: Xiupeng Wang **Copy Editor:** Ping Zhang **Production Editor:** Ping Zhang

Abstract

Bioactive glass (BG) degrades *in vivo*, releasing therapeutic ions and forming an apatite-like phase to repair hard tissues. While many BG-derived materials have been employed clinically, researchers continue to work on improving the physicochemical properties and biological functions of BG due to its inappropriate degradation rate and unsatisfactory bone repair effects. Our previous work revealed that the incorporation of chlorine (Cl) into BG expanded the glass structure, facilitating glass degradation and rapid hydroxyapatite formation. Chloride-containing bioactive glasses (GPCl) showed good osteogenesis effects *in vitro* and *in vivo*. However, the fast degradation rate of GPCl may cause a mismatch between bone formation and glass degradation, limiting its bone repair efficacy. This study incorporated various amounts of magnesium (Mg, 0-20 mol%) into GPCl to regulate its degradation behavior and enhance its bone regeneration ability. Four glasses were synthesized using a melt-quench method. The *in vitro* glass bioactivity was evaluated in Minimum Essential Medium-α (α-MEM), while the *in vivo* osteogenic effect of Mg-doped chloride-containing bioactive glasses (GPMgCl) was investigated on a rat skull critical-size defect and compared with the commercially available bone substitute (Bio-Oss®). Additionally, the blood and main organs of rats were collected to assess the biocompatibility of GPMgCl. Our results

demonstrated that Mg delayed the degradation rate of GPCl and the rate of hydroxyapatite formation while maintaining excellent bioactivity in α-MEM. GPMgCl promoted the expression of osteogenic genes osteocalcin (OCN), bone morphogenetic protein 2 (BMP2), and vascular endothelial growth factor (VEGF), and facilitated the formation of the mineralized nodules. Moreover, it exhibited superior osteogenic effects compared to Bio-Oss® *in vivo*, with GPMg10Cl showing optimal bone regeneration ability. Blood biochemical analyses, blood cell tests, and hematoxylin-eosin staining of organs confirmed the excellent biocompatibility of GPMgCl. Incorporating Mg into GPCl is a promising approach to regulate degradation behavior and enhance osteogenic performance, making GPMgCl a promising bone substitute material to meet future bone repair needs.

Keywords: Bioactive glass, chloride, magnesium, bone regeneration, biocompatibility

INTRODUCTION

Millions of people worldwide lost their teeth due to periodontitis, caries, trauma, and diabetes[1,2]. Tooth loss can lead to occlusion disorders, reduced chewing ability, psychological burden, and systemic diseases such as hypertension and coronary heart disease[3,4]. Dental implantation is the most effective and common method to restore occlusion and function. However, most patients require bone grafts to maintain the height and width of the alveolar bone, which is essential for the success of dental implants[5]. Generally, autografts are the most ideal option due to their composition. However, their limited availability, risk of rejection, infection, and secondary trauma can restrict therapeutic efficacy and lead to the failure of bone implantation[6].

The commercial anorganic bovine bone matrix (Bio-Oss®) is widely used as a bone substitute in dentistry due to its similar structure and porosity to human bone and its protein-free composition[7]. However, the slow degradation rate of Bio-Oss® may limit the space available for bone regeneration[8]. Additionally, Bio-Oss® lacks osteoinductive properties, indicating it requires more time to achieve complete bone regeneration[9]. Therefore, there is an urgent need for synthetic material with biocompatibility osteoconduction, osteoinduction and an appropriate degradation rate to support bone regeneration[10,11]. One promising material is Bioactive glass (BG). BG can degrade to release ions such as Si^{4+}, PO_4^{3-}, and Ca^{2+} and form hydroxyapatite (HAP), the main component of bone[12]. The HAP layer can bind growth factors and promote the attachment of osteoprogenitor cells[13]. Moreover, the released ions from glass can stimulate osteoblast differentiation[14]. Recently, BG has garnered significant attention due to its biocompatibility, bioactivity, and osteogenic ability[15]. Although many commercial BG-derived products such as NovaMin®, MEP®, ERMI®, PerioGlas® and Biogran® have been employed clinically, their degradation behavior and osteogenesis ability have not met expectations[16,17]. Improving and achieving a balance between BG degradation and new bone formation remains a significant challenge.

Incorporating functional elements into BG is an effective approach to modify glass structure, properties and thus its functions[18]. The introduction of strontium (Sr) into BG enhanced the osteogenic ability[19], while increasing phosphorus content reasonably led to more HAP formation and promoted bone formation[20]. Adding copper (Cu) into BG promoted vascularization and antibacterial effects[21]. Chlorine (Cl) is another novel and interesting element that can tune glass properties. Chloride ions, which are abundant in the blood and contribute to two-thirds of the negative charge and one-third of tonicity, are biocompatible and crucial for charge balance and metabolism. Chloride deficiency can lead to metabolic alkalosis and hypokalemia[22]. Chen *et al.*[23,24] developed the first series of chloride-containing bioactive glasses (GPCls) and revealed that the incorporation of chloride expands BG structure, accelerating glass degradation and HAP formation and making GPCl highly bioactive. Additionally, GPCls have been shown to upregulate the expression of osteogenic and angiogenic genes and proteins and enhance bone formation *in vivo*[25]. However, the fast

degradation of GPCls may cause a mismatch between material degradation and bone formation rates, limiting their bone repair efficacy[26,27].

Magnesium (Mg) has been added into 45S5 and a phosphate glass (Mol%: 20Na_2O - 30CaO - 50P_2O_5), and both were found to postpone glass degradation[28,29]. Mg^{2+} is the fourth most abundant cation in the human body, primarily stored in bone tissue and involved in hundreds of biochemical reactions[30], making it important for bone formation and biological functions. Studies have shown that Mg is essential for bone health, with Mg deficiency leading to low bone mineral density and bone inflammation[31]. Hohenbild *et al.*[32] replaced 3 mol% and 6 mol% Ca with Mg in the glass composition ICIE 16 (Mol%: 49.46SiO_2-36.27CaO-6.6Na_2O-1.07P_2O_5-6.6K_2O), resulting in higher expression levels of osseous extracellular matrix-related genes compared to the ICIE 16-BG group. Dai *et al.*[33] synthesized Mg-doped bioactive glass cement (Mg-BGC), demonstrating better osteogenesis and immune regulation performance compared to non-Mg BG cement and calcium sulfate cement *in vitro*. Therefore, given the ability of magnesium to promote BG degradation while facilitating osteogenesis and bone integration, we hypothesized that adding Mg into a GPCl is an effective strategy for tuning its degradation behavior and osteogenic properties, ensuring a balance between material degradation and bone formation.

In this study, we incorporated the Mg into a sodium-free, high phosphorus and Cl-containing BG (composition in Mol%: 30.3SiO_2 - 44.1CaO - 5.0P_2O_5 - 20.6$CaCl_2$) by replacing CaO with MgO and keeping other components constant to further modify the degradation rate and improve the osteogenic ability of GPCl. Mg-doped Cl-containing BG (GPMgCl) with different amounts of content Mg was synthesized by a melt-quench method. The degradation rate of GPMgCl and HAP formation were evaluated using Fourier-Transform Infrared Spectroscopy (FTIR) and Inductively Coupled Plasma - Optical Emission Spectrometer (ICP-OES). The alkaline phosphatase (ALP) activity, mineralized nodule formation, and expression levels of osteogenesis-related genes and proteins were assessed to evaluate the osteogenesis effects of the GPMgCl. In addition, a critical-sized calvarial defect rat model was used to evaluate the bone formation ability of GPMgCl, as skull growth and development are similar to the jaw, both involving intramembranous ossification. Bio-Oss® was used as a positive control *in vivo*. Furthermore, the biocompatibility of GPMgCl was assessed by hematoxylin and eosin (HE) staining and blood analysis. This work focuses on the degradation behavior, osteogenesis, and biocompatibility of GPMgCl, which may aid in the clinical application of novel BG bone substitute materials in the future.

MATERIALS AND METHODS

Glass synthesis

Glasses in the SiO_2-P_2O_5-$CaCl_2$-CaO-MgO system were prepared using the melt-quench method. Briefly, analytical grade SiO_2, P_2O_5, $CaCl_2 \cdot 2H_2O$, $CaCO_3$, and MgO were weighed to achieve a total batch size of 200 g according to the glass compositions [Table 1]. The reagents were mixed thoroughly and melted in a platinum/rhodium crucible at a temperature of 1,470 °C in an electric furnace. After 1 h melting, the glass melt was water quenched rapidly and dried in an oven at 60 °C overnight. Subsequently, 100 g of each glass frit was ground in a Gyro mill for two periods of 7 min and sieved with mesh analytical sieves to obtain glass with different particle sizes.

Bioactivity evaluation in minimum essential medium-α

The glass bioactivity in terms of glass degradation and apatite formation abilities were investigated in Minimum Essential Medium-α (α-MEM). Glass powders with a particle size smaller than 38 μm (75 mg) were dispersed in 50 mL of α-MEM media, resulting in a concentration of 1.5 g/L. All samples were placed in an orbital shaking incubator (IKA®KS, Germany) at 37 °C with an agitation rate of 60 rpm for 6, 24, 72

Table 1. The glass composition in mol%

Glass code	SiO_2	CaO	P_2O_5	MgO	$CaCl_2$
GPMg0Cl	30.3	44.1	5.0	0	20.6
GPMg5Cl	30.3	39.1	5.0	5.0	20.6
GPMg10Cl	30.3	34.1	5.0	10.0	20.6
GPMg20Cl	30.3	24.1	5.0	20.0	20.6

GPMgCl: Mg-doped chloride-containing bioactive glasses.

and 168 h. At each time point, the α-MEM and solids were separated using filter papers with a pore size of 5 to 13 μm.

Apatite formation

The apatite formation ability of GPMgCl in α-MEM was evaluated by FTIR (Bruker, Germany) on the collected solids after filtration. The data were collected in the range of 500 to 1,600 cm^{-1}, as previously described by Chen *et al.*[34].

pH changes and ions release

The pH values of the collected α-MEM were measured using a pH meter (OHAUS, China). Two separate samples from each immersion time point were prepared for all studied glasses. The concentrations of calcium, magnesium, silicon, and phosphorus ions in the α-MEM were quantified using an ICP-OES (PerkinElmer, USA) after dilution by a factor of 2 in deionized water.

Cytotoxicity of glass-conditioned media

The glass-conditioned media was prepared by dispersing 75 mg of glass particles in 50 mL of α-MEM for 72 h. The separated α-MEM was sterilized using a 0.22 μm filter injection syringe and further supplemented with 10% fetal bovine serum and 1% (v/v) penicillin/streptomycin. The MC3T3-E1 cells were cultured in the glass-conditioned media for 1, 3, 5, and 7 days. The media was changed every two days. The cytotoxicity of glass-conditioned media on MC3T3-E1 cells was assessed using a cell counting kit-8 (CCK-8) test according to the manufacturer's instructions, and the absorbance was quantified at 450 nm using an ultraviolet-visible (UV-Vis) Absorption Spectroscopy (BioTerk, USA). The α-MEM supplemented with 10% fetal bovine serum and 1% (v/v) penicillin/streptomycin was used as a control group.

Effect on osteoblasts *in vitro*

ALP staining and activity quantification

After the treatment with glass-conditioned media for 14 days, the cells were washed twice with phosphate-buffered saline (PBS) and then fixed in 4% formaldehyde. The cells were stained using the ALP staining test kit (Beyotime, China). For the quantification of ALP activity, the cells were lysed by three freeze-thaw cycles, and then reacted with 2.5 mg/mL of 4-nitrophenyl phosphate disodium hexahydrate containing 1 mM $MgCl_2$ (pH 9.5) for 1 h. The reaction was stopped with 0.5 mol/L NaOH, and the absorbance was quantified at 405 nm. To promote the osteoblast differentiation, 50 ug/mL ascorbic acid (Sigma, USA), 10 μmol/L beta-glycerophosphate (Sigma, USA), and 10 nmol/L dexamethasone (Sigma, USA) were supplemented into the glass-conditioned media[35].

Alizarin Red S staining and quantification

After culturing with glass-conditioned media for 14 and 21 days, the mineralized nodule formation ability was assessed by Alizarin Red S (ARS) staining. The cells were washed twice with PBS and fixed in a 4% formaldehyde solution. Subsequently, they were rinsed with ddH_2O and stained with 0.5% ARS (pH 4.0)

(Sigma, USA) for 30 min. The quantification of mineralized nodules involved incubation with 10% cetylpyridinium chloride solution (Sigma, USA) for 30 minutes, followed by the measurement of absorbances at 570 nm.

Quantitative real-time polymerase chain reaction

After treatment with glass-conditioned media for 7 and 14 days, the expression levels of osteogenic genes osteocalcin (OCN) and bone morphogenetic protein 2 (BMP2), and angiogenic genes vascular endothelial growth factor (VEGF) were evaluated by real-time polymerase chain reaction (RT-qPCR). RNA was reverse-transcribed into cDNA using ReverTra Ace qPCR RT Master Mix reagents (TOYOBO, Japan) following the manufacturer's instructions. Subsequently, 100 ng of total cDNA was used for RT-qPCR analysis with KOD SYBR® qPCR Mix reagents (TOYOBO, Japan). The relative expression of genes was calculated using the ΔΔCt method with glyceraldehyde-3-phosphate dehydrogenase (GAPDH) as the endogenous reference. Fold change was determined using $2^{-\Delta\Delta Ct}$.

Western blotting

After treatment with glass-conditioned media for 7 and 14 days, cells were lysed using radioimmunoprecipitation assay (RIPA) lysate buffer (Beyotime, China) containing protease inhibitors. The protein concentrations were analyzed using the bicinchoninic acid (BCA) protein assay kit (Thermo Scientific, USA). Equal amounts of protein by weight were subjected to Sodium Dodecyl Sulfate-Polyacrylamide Gel Electrophoresis (SDS-PAGE) and then transferred onto polyvinylidene difluoride (PVDF) membranes (Millipore, USA). The membranes were blocked with 5% bovine serum albumin (BSA) and incubated overnight at 4 °C with primary antibody BMP2 (Abcam, UK) and VEGF (Abcam, UK). Following incubation, membranes were probed with horseradish peroxidase (HRP)-conjugated secondary antibody (Abcam, UK) at room temperature for 1 h. Protein bands were visualized using a Super Sensitive enhanced chemiluminescence (ECL) Luminescence Reagent (Mmeilunbio, DalianChina) and detected with an ECL detection system (Tanon, China). The optical densities of the bands were quantified using Image J software.

In vivo evaluation of bone regeneration ability and biocompatibility

The animal experiment was approved by the Institutional Animal Care and Use Committee (IACUC) of Central South University (Certificate No.CSU-2022-0189). Eight-week-old Sprague-Dawley (SD) rats weighing around 250 g were used in the following *in vivo* studies.

Surgical procedures

The critical-size calvarial defect model was used to assess the bone formation abilities of GPMgCl and Bio-Oss®, since the skull and jawbone are both flat bone and have the same development and growth type, which is intramembranous ossification. Thirty 8-week-old male SD rats were randomly divided into six groups: control, Bio-Oss®, GPMg0Cl, GPMg5Cl, GPMg10Cl, and GPMg20Cl. After anaesthetization, two critical-size calvarial defects (5 mm in diameter) were created using a dental implant drill and grafted with or without different grafting materials, and the rats were sacrificed 8 weeks after implantation. The particle size of Bio-Oss® and GPMgCl BG series used *in vivo* ranged from 250 to 1,000 μm. Each group had five replicated defects (n = 5).

The bone regeneration ability in vivo

Micro-computed tomography

The evaluation of new bone formation in the harvested skull bones at week 8 post-surgery was conducted using the Hiscan XM Micro-Computed Tomography (Micro-CT) (Suzhou Hiscan Information Technology Co., Ltd, China). The X-ray tube settings were 80 kV and 100 μA, and images were acquired at a resolution of 25 μm. A 0.5° rotation step through a 360° angular range with 50 ms exposure per step was employed. The images were reconstructed using Hiscan Reconstruct software (Version 3.0, Suzhou Hiscan Information Technology Co., Ltd, China), and the bone volume fraction (BV/TV) was analyzed with Hiscan Analyzer software (Version 3.0, Suzhou Hiscan Information Technology Co., Ltd).

Histological analysis of bone

Skull samples after the computed tomography (CT) scan were decalcified by immersing in 10 % ethylenediaminetetraacetic acid (EDTA) decalcifying fluid (Biofroxx, Germany) for 4 weeks. Subsequently, 5 μm-thick sections were prepared from the tissues for histological analysis. Hematoxylin and eosin (H&E) staining and Masson's Trichrome staining were performed to assess new bone and collagen formation. Immunohistochemistry (IHC) was conducted to analyze the expression levels of BMP2 protein (antibody 1:100) within the defect area.

Biocompatibility evaluation

Blood cell and blood biochemistry analysis

The rats with two defects grafted with different materials are not suitable for investigating the biocompatibility of a single material. Therefore, in this study, rats with one defect grafted with a material and the other left empty were used to evaluate the biocompatibility of the specific material being tested. In order to evaluate the possibility of combining commercially available products with developed bioactive glasses (BGs), the rats grafted with either Bio-Oss® and GPMg0Cl or Bio-Oss® and GPMg20Cl were also studied. Moreover, rats with two defects without grafting materials were used as the control group. Blood samples were collected at 7 days and 8 weeks post-implantation via the caudal vein. The blood was centrifugated at 3000rpm, and the serum was analyzed for level of total protein (TP), albumin (ALB), creatinine (CREA), and blood urea nitrogen (BUN). Whole blood, after anticoagulation, was used to determine levels of white blood cells, red blood cells, and hemoglobin[36].

HE staining of main organs

Upon sacrifice, these organs were fixed in 4% paraformaldehyde for 48 h and embedded in paraffin to prepare 5 μm thick sections. Subsequently, sections were stained with HE to detect any pathological changes.

RESULTS AND DISCUSSION

Bioactivity evaluation in α-MEM

As shown in Supplementary Figure 1, all the studied BGs were largely amorphous. The low-intensity crystalline phase observed in GPMg0Cl and GPMg5Cl is highly likely due to reactions with water during quenching. Figure 1A shows the FTIR spectra of GPMg0Cl after immersion for 6, 24, 72, and 168 h in α-MEM. At 6 h, the intensity of the non-bridging oxygen (NBO) band at 920 cm^{-1} decreased notably, indicating the degradation of GPMg0Cl. The appearance of the typical bands at 560 cm^{-1}, 600 cm^{-1}, and 1,030 cm^{-1} suggested a rapid apatite-like phase formation. In addition, the intensity of the Si-O(NBO) band at about 920 cm^{-1} was stronger in the glasses with higher Mg content. By 72 h, a band at 790 cm^{-1} corresponding to the Si-O-Si bond was observed, indicating the formation of silicon gel. These results

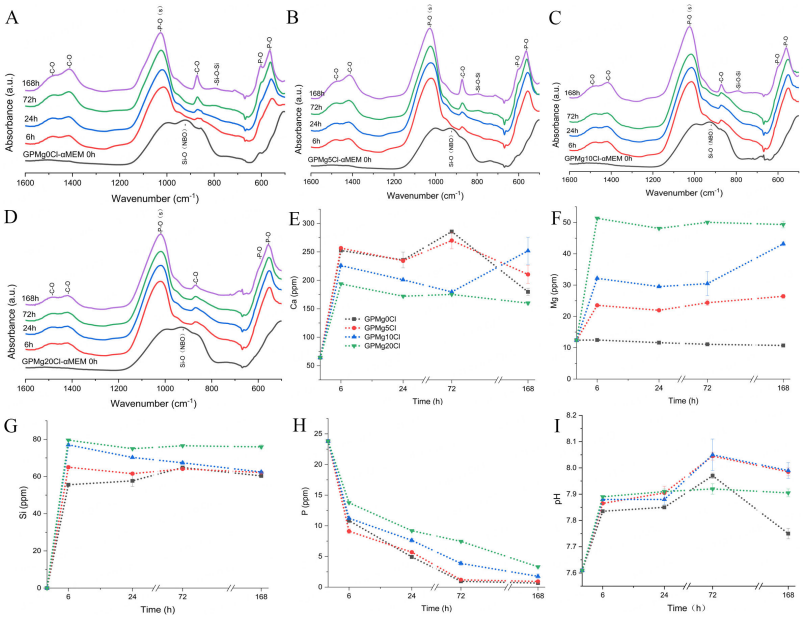

Figure 1. Bioactivity evaluation of GPMgCl in α-MEM up to 168 h of immersion: (A-D) FTIR spectra of GPMg0Cl, GPMg5Cl, GPMg10Cl, and GPMg20Cl immersed in α-MEM for 0, 6, 24, 72, and 168 h, respectively; (E-H) Concentration of Ca, Mg, Si, and P ions in α-MEM after GPMg0Cl, GPMg5Cl, GPMg10Cl, and GPMg20Cl immersion for 6, 24, 72, and 168 h; (I) pH variation at 6, 24, 72, and 168 h. The ion concentrations and pH value of 0 h represent the initial ion concentrations and pH of α-MEM. α-MEM: Minimum essential medium-α; FTIR: Fourier-transform infrared spectroscopy; GPMgCl: Mg-doped chloride-containing bioactive glasses.

demonstrate a fast degradation and apatite formation rate of GPMg0Cl. As the immersion time increased to 168 hours, the apatite bands became more pronounced. With increasing Mg content in the BGs, the time to first observe the apatite split bands and the disappearance of the NBO band was delayed, suggesting that the presence of Mg slowed down the rate of BG degradation and HAP formation [Figure 1B-D], due to the smaller radius and stronger cation field strength of Mg^{2+}, resulting in a denser and stronger glass structure[28,29]. The FTIR spectra [Supplementary Figure 2] further confirm that GPMg0Cl and GPMg5Cl exhibited faster degradation and apatite formation rates compared to the typical BG 45S5, while GPMg10Cl and GPMg20Cl showed slower degradation and HAP formation rates than 45S5. However, all the studied BGs remained highly bioactive, with apatite detected within 168 h and 14 days [Supplementary Figure 3] in α-MEM.

Supplementary Figure 4 presents the normalized FTIR spectra of collected glass powder after 72 h immersion. It is clear that the intensity of Si-O(NBO) band at about 920 cm^{-1} was stronger in the glasses with higher Mg content; meanwhile, the Si-O-Si band at 790 cm^{-1}, associated with Si-gel formation, was observed in the spectra of GPMg0Cl and GPMg5Cl but not in GPMg10Cl and GPMg20Cl. These findings indicate that the incorporation of Mg delays glass degradation and probably Si-gel formation.

The changes in ion concentration and pH of α-MEM were measured to further investigate the bioactivity of the GPMgCl. Figure 1E-H shows the concentrations of Ca, Mg, Si, and P in α-MEM after BG immersion for 6, 24, 72, and 168 h. The data at 0 hours represent the original ion concentrations in the α-MEM. The concentration of Ca^{2+} [Figure 1E] in all BGs increased rapidly from 0 to 6 h, suggesting that the rate of degradation was faster than the HAP formation. From 6 to 24 h, the concentration of Ca^{2+} decreased, indicating that the HAP formation rate was faster than the BG degradation rate. The concentration of Ca^{2+} in GPMg0Cl and GPMg5Cl increased from 24 to 72 h, then decreased from 72 to 168 h. However, the trend

of Ca^{2+} concentration in GPMg10Cl was contrary to those of GPMg0Cl and GPMg5Cl, while GPMg20Cl showed an unchanged Ca^{2+} concentration from 24 to 168 h. Within 72 h of immersion, the percentage of Ca released decreased with increasing Mg content in the glass compositions [Supplementary Figure 5], suggesting incorporation of Mg delays glass degradation, which shows a good agreement with FTIR results [Supplementary Figure 4]. The concentration of Mg^{2+} in α-MEM was 12 ppm [Figure 1F]. The rapid increase in Mg^{2+} within the first 6 h demonstrated the fast degradation of GPMg5Cl, GPMg10Cl, and GPMg20Cl. The concentration of Mg^{2+} stabilized after 72 h in GPMg5Cl (about 25 ppm), while it continued to increase in GPMg10Cl (over 30 ppm), implying that GPMg10Cl continued to degrade after 72 h. The slight change in Mg^{2+} concentration in GPMg20Cl (about 50 ppm) could be due to its slowest degradation rate, as evidenced by the extremely asymmetric peak at 1030 cm^{-1} [Figure 1D], indicating incomplete degradation of GPMg20Cl.

It is apparent that the Si^{4+} concentration [Figure 1G] had a positive correlation with the Mg content of BGs at 6 h, suggesting that high Mg^{2+} concentration may affect glass degradation and the Si-gel formation. This is also evident in the FTIR spectrum of GPMg20Cl [Figure 1D], which shows the highest peak intensity at 920 cm^{-1} but the lowest intensity at 790 cm^{-1} in GPMg20Cl. The Si concentration reached saturation after 72 h of immersion and no significant changes were observed across all groups. Interestingly, Si concentrations in GPMgCl were higher than in Mg-free glass. The Si-O-Si band at 790 cm^{-1}, associated with Si-gel formation, was observed in the spectra of GPMg0Cl and GPMg5Cl but not in GPMg10Cl and GPMg20Cl after 72 h of immersion [Supplementary Figure 4]. The X-ray Diffraction (XRD) results [Supplementary Figure 6] also confirm Si-gel formation, showing a characteristic Si-gel signal at 20-22 (2θ) in GPMg0Cl at 72 h, but not in GPMg20Cl. These observations suggest that Mg delays Si-gel formation, resulting in higher Si concentrations in solutions with higher Mg content in glass compositions.

The decrease in P^{5+} concentration is attributed to the consumption of PO_4^{3-} for HAP formation. Moreover, the phosphate concentration in high Mg-containing BGs is higher than that in lower ones, implying high Mg content significantly delayed HAP formation. However, the HAP formation in GPMg5Cl was not significantly affected by the relatively low concentration of Mg^{2+}. Mg released from BG could potentially be incorporated into the reactive apatite layer, given the remarkable ability of apatites to accommodate a wide range of substitutional ions. The use of ^{31}P magic angle spinning-nuclear magnetic resonance (MAS-NMR) and ^{25}Mg MAS-NMR would indeed be valuable in investigating such substitutions. However, it is worth noting that obtaining a good signal for ^{25}Mg MAS-NMR can be particularly challenging, especially when the level of Mg substitution is low.

As the BGs degraded, the pH of α-MEM increased at 6 hours in all groups and continued to increase from 24 to 72 h, while the pH in GPMg20Cl remained stable after 6 h [Figure 1I]. The increase in pH was caused by the BG degradation, which led to the exchange of metal cations (Ca^{2+} and Mg^{2+}) from BGs with H^+ in the media, resulting in an increase in OH^- concentration[37]. The formation of HAP consumes OH^-, causing a decrease in pH. The rapid increase in pH indicated fast degradation of BGs, while the stable pH in GPMg20Cl suggested a slow glass degradation and apatite formation process, and a relatively balance between the glass degradation rate and HAP formation rate. From 72 to 168 h, the pH in GPMg0Cl, GPMg5Cl, and GPMg10Cl decreased, with GPMg0Cl showing the lowest pH value, indicating the most HAP formation in the GPMg0Cl group during this period. This result is also evident from the most significant Ca consumption [Figure 1E] in GPMg0Cl from 72 to 168 h. Since abundant ions are present in α-MEM, further investigation into the relationship between GPMgCl structure and bioactivity needs to be conducted in Tris buffer solution, which lacks ions that could affect the degradation of glasses and HAP formation.

Cell culture and cytotoxicity of glass-conditioned culture media

As shown in Supplementary Figure 7, none of the glass-conditioned culture media were cytotoxic to the MC3T3-E1 cells compared to the control group. Although on day 1, the viability of MC3T3-E1 cells in the GPMg20Cl group decreased slightly compared to the other experimental groups, there was no significant difference compared with the control. This may be due to the low cell density on day 1 and the highest concentration of Mg in the GPMg20Cl group, as seen in Figure 1F, resulting in low viability[38]. However, as the cells continued to proliferate, no differences were observed among the groups.

In vitro osteogenic effects

ALP activity

As a marker of osteogenic differentiation, the activity level of ALP represents osteogenic differentiation ability[39]. Figure 2A shows that GPMg5Cl, GPMg10Cl, and GPMg20Cl significantly enhanced the ALP activity of MC3T3-E1 cells, whereas GPMg0Cl did not show a distinct enhancement in the ALP activity compared to the control group on day 14 [Figure 2B]. This result indicates that the environment created by GPMgCl degradation, likely due to the released Mg^{2+}, upregulated the expression of ALP, thereby promoting osteoblast differentiation. However, there was no significant difference in ALP activity among GPMg5Cl, GPMg10Cl, and GPMg20Cl. Zhong *et al.*[40] synthesized a series of Mg-doped BGs by replacing 6, 20, and 36 mol% Ca with Mg in a glass composition of 60.0 SiO_2 - 4.0 P_2O_5 - 36.0 CaO (Mol%) to analyze the effect of the Mg-BG on mineralization and odontogenesis ability of human dental pulp stem cells (hDPSCs). The Mg-BG significantly upregulated the expression of ALP on days 7 and 14. There was no significant difference among the different Mg content groups on day 14, which is consistent with our results.

ARS staining

The formation of mineralized nodules represents osteogenic and mineralized abilities[41]. As shown in Figure 2C and D, the formation of mineralized nodules was significantly promoted in all the BG groups compared to the control after 14 and 21 days. On day 14, the formation of mineralized nodules followed the decreasing order: GPMg10Cl, GPMg5Cl, GPMg20Cl, GPMg0Cl, and control. The trend on day 21 was generally the same as on day 14. However, the mineralized nodules in GPMg0Cl were more numerous than in GPMg20Cl on day 21. This implies that a high concentration of Mg may negatively impact bone mineralization and osteogenesis. The GPMg10Cl group showed the best mineralization at each time point of interest. Although the mineralized nodule formation in GPMg20Cl was less than in GPMg0Cl on day 21, it was still better than the control group. Chu *et al.*[42] reported that a high level of Mg can stimulate ALP activity but disrupt bone mineralization.

Osteogenesis-related gene expression

To further evaluate the effect of GPMgCl on osteogenesis, RT-qPCR was conducted to assess the expression levels of osteogenesis-related genes in MC3TE-E1 cells treated with BG-conditioned culture media. On day 7, the expression of OCN was significantly upregulated in all the BG groups in the following decreasing order: GPMg5Cl, GPMg10Cl, GPMg20Cl, GPMg0Cl, and control [Figure 3A]. On day 14, the highest OCN gene expression was observed in the GPMg10Cl group, followed by GPMg5Cl, GPMg0Cl, GPMg20Cl, and control. OCN is a key gene involved in bone mineralization and alignment of HAP, enhancing bone density and strength. Incorporating Mg into GPCl significantly promoted OCN expression, indicating that Mg is important for bone mineralization. The expression level of the runt-related transcription factor 2 (RUNX2) gene is shown in Figure 3B. RUNX2 was upregulated in the GPMg0Cl, GPMg5Cl, and GPMg10Cl groups on day 7, with no significant difference between GPMg20Cl and the control. On day 14, all the BG groups had lower RUNX2 levels compared to the control. This is due to the fact that RUNX2 is a key transcription factor in the early stages of osteoblast differentiation, and its expression decreases in mature osteoblasts[43,44]. VEGF is a key gene involved in angiogenesis, significantly promoting angiogenesis and providing adequate

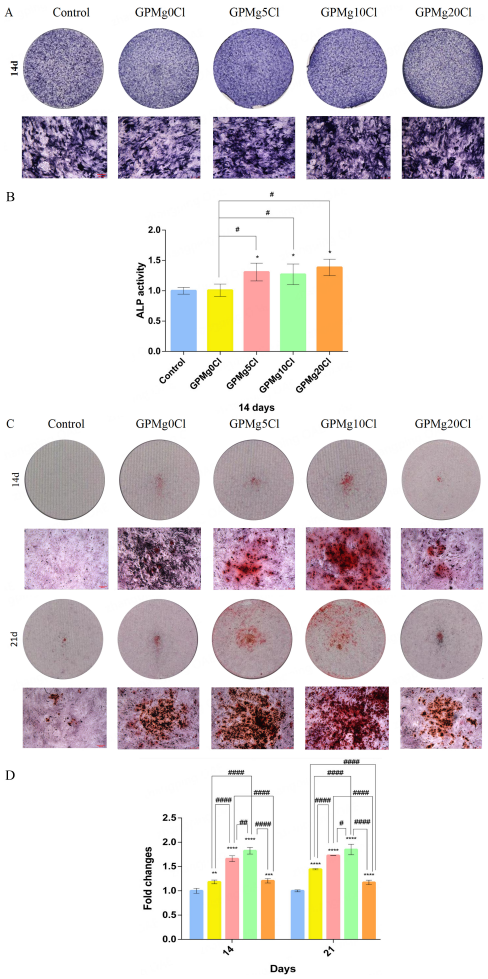

Figure 2. Osteogenesis ability evaluation after culturing in glass-conditioned culture media for different time points. (A) ALP staining quantification of MC3T3-E1 at 14 days (n = 4); (B) Quantification of ALP activity at 14 days; (C) Alizarin Red S staining at 14 and 21 days (n = 3); (D) Quantification of mineralized nodule formation at 14 and 21 days. Data are presented as the mean ± SD. *P < 0.05, **P < 0.01, ***P < 0.005, ****P < 0.0001, compared with the control group. #p < 0.05, ##P < 0.01, ###P < 0.005, ####P < 0.0001, compared with each experimental group. The bar represents 250 μm, and the values were normalized by comparison with the control group. ALP: Alkaline phosphatase.

nutrition for bone formation. Additionally, VEGF was found to directly promote osteoblast differentiation and bone repair[45]. Our previous study found that Cl-containing BG promoted VEGF expression to stimulate osteogenesis[25]. In this study, VEGF gene expression was upregulated in GPMg0Cl, GPMg5Cl, and GPMg10Cl groups compared to the control group on day 7 [Figure 3C]. However, on day 14, there was no difference in VEGF gene expression among all the groups.

Osteogenesis-related protein expression

The expression and quantification of BMP2 protein are shown in Figure 3D and E, respectively. On day 7, BMP2 protein expression was upregulated in the GPMg5Cl and GPMg10Cl groups. On day 14, compared to the control group, the expression level of BMP2 protein was further increased, with the GPMg5Cl group showing the most significant upregulation. On day 7, VEGF protein expression was promoted in the GPMg5Cl and GPMg10Cl groups [Figure 3F and G], while there was no significant difference among the groups on day 14. The GPMg20Cl group showed no significant upregulation effect on BMP2 and VEGF protein expression, indicating that the large amount of Mg generated by dissolving GPMg20Cl in α-MEM

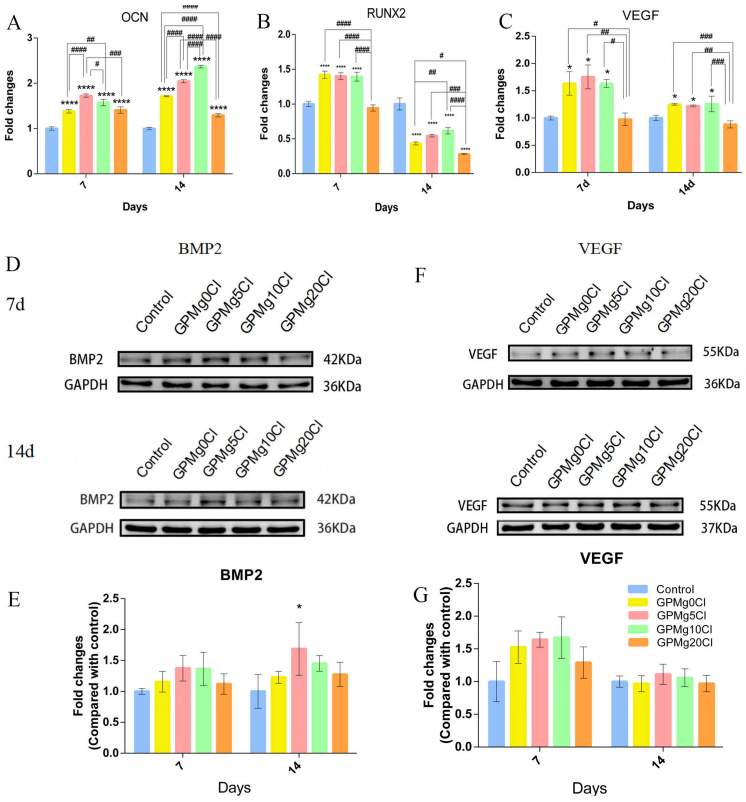

Figure 3. Osteogenesis-related gene and protein expression levels: (A-C) Gene expression of OCN, RUNX2, and VEGF in MC3T3-E1 cells following treatment with BG-conditioned culture media for 7 and 14 days, respectively (n = 3); (D) and (F) Representative images of BMP2 and VEGF protein expression in MC3T3-E1 cells on days 7 and 14; (E) and (G) Quantification of BMP2 and VEGF protein expression levels by ImageJ. Data are presented as the mean ± SD (n = 3). $^{*}P$< 0.05, $^{**}P$ < 0.01, $^{***}P$< 0.005, $^{****}P$< 0.0001, compared with control group. $^{\#}P$ < 0.05, $^{\#\#}P$ < 0.01, $^{\#\#\#}P$ < 0.005, $^{\#\#\#\#}P$ < 0.0001, compared with each experimental group. OCN: Osteogenic genes osteocalcin; BMP2: Bone morphogenetic protein 2; VEGF: Vascular endothelial growth factor; BG: Bioactive glass; RUNX2: Runt-related transcription factor 2.

may have an adverse effect on osteogenesis. Li *et al.*[46] incorporated Mg into nanoporous titanium and found that the presence of Mg coating significantly increased mineralized nodule formation. However, as the Mg content increased, mineralized nodule formation was inhibited by excessive Mg. This suggests that a too-high concentration of Mg may harm the growth of osteoblasts.

In vivo osteogenic effects

Micro-CT analysis of new bone formation

Figure 4A shows the representative images of bone defect after 8 weeks of implantation. It is clear that the control group exhibited the largest defect size. The size of defects grafted with either Bio-Oss® or BGs reduced significantly. Generally, a small amount of residual BG granules was present in the defects at week 8, particularly in the GPMg20Cl group. In the Bio-Oss® group, a significant amount of residual Bio-Oss® granules and limited integration were observed within the defect, with the interface between Bio-Oss® and bone remaining visible. These observations are attributed to the limited degradation and osteoinduction abilities of Bio-Oss®. All GPMgCl groups showed varying but desirable degrees of degradation and integration with host bone, with the GPMg10Cl group exhibiting complete closure of the defect. In addition, the interface between the glass and the host bone was barely identifiable, indicating excellent osseointegration, which is necessary for successful implantation[47]. Figure 4B presents the quantitative analysis of newly formed bone. The volume of newly formed bone in the Bio-Oss® group was higher than in

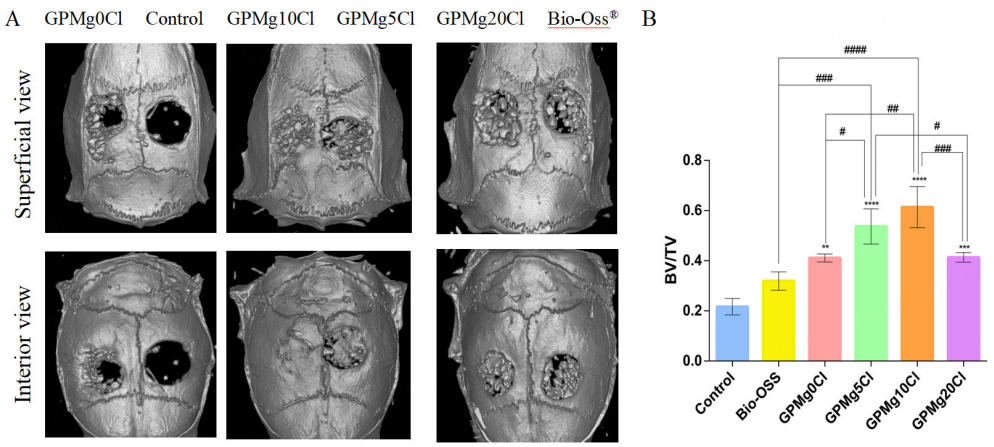

Figure 4. Micro-CT evaluates the bone formation ability of GPMgCl and Bio-Oss® (A) The representative images of calvarial defects in rats implanted with GPMgCl or Bio-Oss® for 8 weeks; (B) The value of BV/TV in every group at week (n = 5). Micro-CT: Micro-computed tomography; GPMgCl: Mg-doped chloride-containing bioactive glasses; Bio-Oss®: Anorganic bovine bone matrix; BV/TV: Bone volume/total volume.

the control, but lower than in the GPCls. The volume of newly formed bone increased with the Mg content in the glass from 0 to 10 mol%. Although the BV/TV value in GPMg20Cl was lower than that in the GPMg10Cl, it was still higher than in the control group. Cheng *et al.*[48] also found that grafting Bio-Oss® in a rat mandible defect showed some new bone formation, but no direct connection between the granules and the surrounding bone, suggesting that a lack of osteoinduction impairs osseointegration.

Histology analysis

The two critical-size skull defect model is a well-established method for studying bone defects and regeneration, as well as potential interactions between the two defects when using different graft materials. To minimize such interactions, we ensured that the histological analysis (including HE, Masson, and IHC staining) focused on bone tissues located far from the midline between the two defects. This approach was intended to avoid any contamination from the adjacent defect site. Figure 5A shows the HE staining results of the interface between bone and grafting materials after 8 weeks. In the control group, there was a small amount of new bone formation, and the defect was mainly filled with disorder and funicular fibers. Bio-Oss® promoted a small amount of new bone formation in the defect area. The GPMgCl group, especially in the GPMg10Cl and GPMg5Cl, exhibited a large amount of compact and lamellar bone formation. Additionally, some pores were observed in the tissue of the defect area, likely caused by the material granules. When the granules were implanted into the defect, cells clustered and adhered to the granules, forming the fibers and collagen. As cell proliferation, differentiation, and mineralized matrix secretion occurred, new bone tissue grew more extensively. This process requires the material to degrade to provide more space for bone formation, indicating that an appropriate degradation rate is necessary for bone regeneration[49]. The largest pores, surrounded by fibrous connective tissue, were observed in the Bio-Oss® group due to its slowest degradation rate[50]. To further analyze the composition of the tissue in the defect area, Masson staining was conducted. As shown in Figure 5B, a large amount of the red-stained connective fiber tissue was present in the control and Bio-Oss® groups. In contrast, the defect area in the GPMgCl groups was composed of blue-stained collagen, the main organic composition of bone. Moreover, the newly formed bone in the GPMgCl groups showed signs of maturation, as demonstrated by the mixed blue and red staining of bone[51,52].

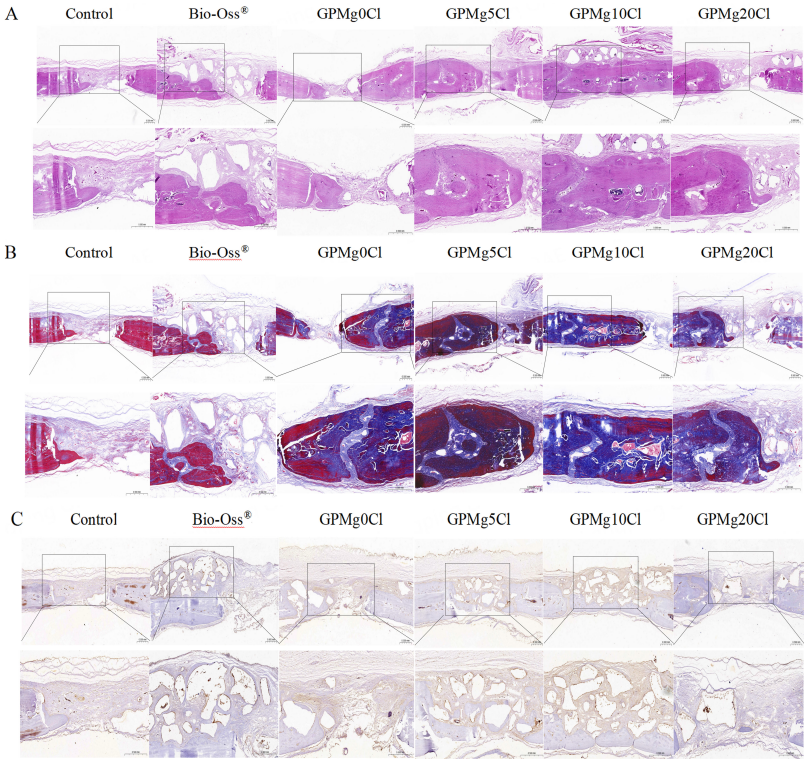

Figure 5. (A) Representative images of HE staining and (B) Masson staining of the interface between the host bone and the materials; (B) Representative immunohistochemistry images of BMP2 between the material granules and tissue. The bar represents 500 μm. HE: Hematoxylin and eosin; BMP2: Bone morphogenetic protein 2.

BMP2 is a crucial growth factor for bone formation[53]. Figure 5C shows the BMP2 expression level in the defect area. In the control and Bio-Oss® groups, immune-complex deposition was barely detectable, indicating low levels of BMP2. In contrast, the GPMg0Cl, GPMg5Cl, and GPMg10Cl groups exhibited a large amount of BMP2. Sahin *et al.*[54] found that Mg^{2+} promotes BMP2 levels in high-fat-fed rats by regulating the BMP2/RUNX2 signaling pathway. However, the GPMg20Cl group showed low BMP2 expression levels, consistent with the western blot results. Some researchers have also reported the negative effects of sustained high doses of Mg release on bone repair[42,46,55,56]. According to these and our data, although Mg is a well-accepted osteogenesis-promoting element, the release dose and content of Mg in bone regeneration materials should be appropriate.

Biocompatibility evaluation

Blood cell and blood biochemistry analysis

Blood collected via the caudal vein was used to further assess the biocompatibility of GPMgCl. Data from day 0 were collected before the surgical procedures and implantation. After 7 days of implantation, white cell counts had slightly increased in all groups, indicating mild inflammation caused by the surgical operation [Table 2]. The control group showed the most significant increase, likely due to the trauma from the bone defect operation. The implantation of GPMgCl did not cause notable inflammation. By 8 weeks, white cell counts had decreased to normal levels. Red cell and hemoglobin levels showed no significant differences compared to the control at all time points. These results suggest that GPMgCl did not impair the hemopoietic system. Table 3 shows the biochemical indices of rats at different time points. The TP, ALB, BUN, and CREA data also suggest that GPMgCl did not affect liver and kidney functions[57,58]. Combining these data with the HE staining of organs, it is apparent that the GPMgCl is biocompatible.

Table 2. Blood cell test of rats before surgery (day 0) and after implanted with control, Bio-Oss®, GPMg0Cl, GPMg5Cl, GPMg10Cl, GPMg20Cl, and mixed groups on day 7 and at week 8

Items	Blood cells								
	White cell (10^9/L)			Red cell (10^{12}/L)			Hemoglobin (g/L)		
Groups	0 d	7 d	8 w	0 d	7 d	8 w	0 d	7 d	8 w
Control	7.44	13.84	14.12	8.71	7.66	8.88	167	145	177
Bio-Oss®	17.07	17.04	6.01	8.44	7.98	5.35	160	149	108
GPMg0Cl	9.53	10.99	10.61	8.52	8.91	8.25	159	163	162
GPMg5Cl	18.00	13.69	10.03	8.83	8.78	9.35	158	153	172
GPMg10Cl	11.05	13.79	9.98	8.88	8.22	7.63	165	148	144
GPMg20Cl	10.31	14.69	13.46	7.62	7.7	8.18	142	141	157
Bio-Oss® and GPMg0Cl	10.05	8.35	9.49	6.61	6.41	9.09	123	117	172
Bio-Oss® and GPMg20Cl	15.43	11.39	20.19	8.51	7.64	8.73	159	142	167

GPMgCl: Mg-doped chloride-containing bioactive glasses; Bio-Oss®: Anorganic bovine bone matrix.

Table 3. The biochemical indices TP, ALB, BUN, and CREA level among groups of rats before surgery (day 0) and after implanted with control, Bio-Oss®, GPMg0Cl, GPMg5Cl, GPMg10Cl, GPMg20Cl, and mixed groups on day 7 and at week 8

Items	Blood biochemistry											
	TP (g/dL)			ALB (g/dL)			BUN (mg/dL)			CREA (mg/dL)		
Groups	0 d	7 d	8 w	0 d	7 d	8 w	0 d	7 d	8 w	0 d	7 d	8 w
Control	8.7	6.5	7.7	5	3.2	3.7	18	9	17	0.1	0.5	0.5
Bio-Oss®	7.3	6.6	12	4.4	3.4	4.7	18	16	16	0.5	0.5	0.7
GPMg0Cl	7.3	6.7	10.7	4.4	3.9	3.2	22	14	17	0.2	0.2	0.5
GPMg5Cl	8.2	7.4	10.1	4.8	4.2	4.3	17	13	16	0.1	0.2	0.5
GPMg10Cl	7.1	6.6	9.6	4.4	3.4	4.5	17	13	20	0.5	0.5	0.5
GPMg20Cl	6.6	6.7	7.7	4	3.3	5.7	19	18	21	0.5	0.5	0.6
Bio-Oss® and GPMg0Cl	7.8	9	6	4.8	5.2	5.3	19	15	17	0.1	0.1	0.8
Bio-Oss® and GPMg20Cl	7.1	3.4	7.7	4.4	3.4	3.9	19	15	20	0.4	0.4	0.6

GPMgCl: Mg-doped chloride-containing bioactive glasses; TP: Total protein; ALB: Albumin; CREA: Creatinine; Bio-Oss®: Anorganic bovine bone matrix.

HE staining of main organs

To investigate the biocompatibility of GPMgCl, we collected the cerebrum, heart, liver, lung, and kidney from rats after 8 weeks of material implantation [Figure 6]. There were no signs of pathology in the organs. In addition, the structure of the cerebrum in the GPMgCl groups was similar to that in the control and Bio-Oss® groups, indicating good biocompatibility of GPMgCl, as it had direct contact with the cerebrum for 8 weeks. The heart, liver, lung, and kidney also showed no obvious histomorphological changes, demonstrating that GPMgCl had no systemic toxicity[59,60].

CONCLUSIONS

In this study, we synthesized the GPMgCl with Mg content ranging from 0 to 20 %mol. The incorporation of Mg delayed the HAP formation and degradation rate of GPMgCl, while all the GPMgCl exhibited good bioactivity in α-MEM. The *in vitro* osteogenesis results revealed that an appropriate amount of Mg can promote osteogenic differentiation and mineralized nodule formation, whereas excessively high Mg concentrations weaken the osteogenesis effect. The *in vivo* study demonstrates the superior bone regeneration ability of GPMgCl than Bio-Oss®, with GPMg10Cl showing the best bone formation effect. Moreover, biocompatibility investigations reveal that Mg-doped GPCls are biocompatible. GPMg10Cl is a

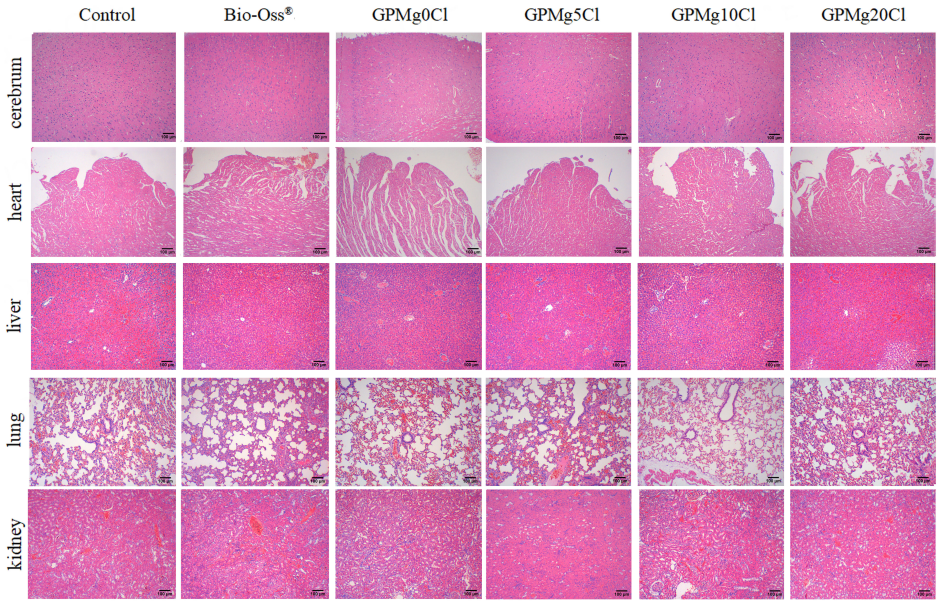

Figure 6. HE staining of the cerebrum, heart, liver, lung, and kidney of the control, Bio-Oss®, GPMg0Cl, GPMg5Cl, GPMg10Cl, and GPMg20Cl groups after 8 weeks of implantation. The bar represents 100 μm. HE: Hematoxylin and eosin; GPMgCl: Mg-doped chloride-containing bioactive glasses; Bio-Oss®: Anorganic bovine bone matrix.

promising bone substitute that addresses the high demand for bone regeneration. Future studies should focus on elucidating the mechanisms by which Mg-doped GPCls promote bone formation and systematically evaluating their biocompatibility in large animals.

DECLARATIONS

Acknowledgments

This study was supported by the Changsha Prominent Young Innovators Program (kq2305026), the Science and Technology Talent Lifting Project of Hunan Province (2023TJ-N18), Huxiang Youth Talent Program of Hunan Province of China (2020RC3064), and Furong Scholar of the Hunan Provincial Department of Education (202058).

Authors' contributions

Experiment implementation, data acquisition and interpretation, statistical analyses, manuscript writing: Ouyang, Z.
In vivo study: Li, P.; Ru, X.; Liu, L.
Glass fabrication: Shah, P.
Study design, manuscript review and editing: Liu, O.
Glass design, discussion, manuscript revision: Hill, R.
Glass design, data interpretation, conceptualization, manuscript review and editing: Chen, X. (Xiaohui Chen)
Conceptualization, methodology, data interpretation, manuscript writing, review and editing, supervision, and funding acquisition: Chen, X. (Xiaojing Chen)

Availability of data and materials

The rata data supporting the findings of this study are available within this Article and its Supplementary Materials. Further data are available from the corresponding authors upon reasonable request.

Financial support and sponsorship

This study was supported by the Changsha Prominent Young Innovators Program (kq2305026), the Science and Technology Talent Lifting Project of Hunan Province (2023TJ-N18), Huxiang Youth Talent Program of Hunan Province of China (2020RC3064), and Furong Scholar of the Hunan Provincial Department of Education (202058).

Conflicts of interest

All authors declared that there are no conflicts of interest.

Ethical approval and consent to participate

The animal experiment was approved by the Institutional Animal Care and Use Committee (IACUC) of Central South University (Certificate No.CSU-2022-0189).

Consent for publication

Not applicable.

REFERENCES

1. Dantas, T. A.; Carneiro, N. J. P.; Alves, J. L.; Vaz, P. C. S.; Silva, F. S. In silico evaluation of the stress fields on the cortical bone surrounding dental implants: comparing root-analogue and screwed implants. *J. Mech. Behav. Biomed. Mater.* **2020**, *104*, 103667. DOI PubMed
2. Smith, E. E.; Angstadt, S.; Monteiro, N.; Zhang, W.; Khademhosseini, A.; Yelick, P. C. Bioengineered tooth buds exhibit features of natural tooth buds. *J. Dent. Res.* **2018**, *97*, 1144-51. DOI PubMed PMC
3. Janto, M.; Iurcov, R.; Daina, C. M.; et al. Oral health among elderly, impact on life quality, access of elderly patients to oral health services and methods to improve oral health: a narrative review. *J. Pers. Med.* **2022**, *12*, 372. DOI PubMed PMC
4. Xu, K.; Yu, W.; Li, Y.; et al. Association between tooth loss and hypertension: a systematic review and meta-analysis. *J. Dent.* **2022**, *123*, 104178. DOI
5. Schröter, L.; Kaiser, F.; Küppers, O.; et al. Improving bone defect healing using magnesium phosphate granules with tailored degradation characteristics. *Dent. Mater.* **2024**, *40*, 508-19. DOI
6. Sivakumar, P. M.; Yetisgin, A. A.; Demir, E.; Sahin, S. B.; Cetinel, S. Polysaccharide-bioceramic composites for bone tissue engineering: a review. *Int. J. Biol. Macromol.* **2023**, *250*, 126237. DOI PubMed
7. Fujisawa, K.; Akita, K.; Fukuda, N.; et al. Compositional and histological comparison of carbonate apatite fabricated by dissolution-precipitation reaction and Bio-Oss®. *J. Mater. Sci. Mater. Med.* **2018**, *29*, 121. DOI
8. Rohr, N.; Brunner, C.; Bellon, B.; Fischer, J.; de, W. M. Characterization of a cotton-wool like composite bone graft material. *J. Mater. Sci. Mater. Med.* **2022**, *33*, 61. DOI PubMed PMC
9. Huh, J. B.; Yang, J. J.; Choi, K. H.; et al. Effect of rhBMP-2 immobilized anorganic bovine bone matrix on bone regeneration. *Int. J. Mol. Sci.* **2015**, *16*, 16034-52. DOI PubMed PMC
10. Wang, S.; Li, R.; Xia, D.; et al. The impact of Zn-doped synthetic polymer materials on bone regeneration: a systematic review. *Stem. Cell. Res. Ther.* **2021**, *12*, 123. DOI PubMed PMC
11. Ciszyński, M.; Dominiak, S.; Dominiak, M.; Gedrange, T.; Hadzik, J. Allogenic bone graft in dentistry: a review of current trends and developments. *Int. J. Mol. Sci.* **2023**, *24*, 16598. DOI PubMed PMC
12. Müller, V.; Djurado, E. Microstructural designed S58 bioactive glass/ hydroxyapatite composites for enhancing osteointegration of Ti6Al4V-based implants. *Ceram. Int.* **2022**, *48*, 35365-75. DOI
13. Ryan, E. J.; Ryan, A. J.; González-Vázquez, A.; et al. Collagen scaffolds functionalised with copper-eluting bioactive glass reduce infection and enhance osteogenesis and angiogenesis both *in vitro* and *in vivo*. *Biomaterials* **2019**, *197*, 405-16. DOI
14. Polo-Montalvo, A.; Casarrubios, L.; Serrano, M. C.; et al. Effective actions of ion release from mesoporous bioactive glass and macrophage mediators on the differentiation of osteoprogenitor and endothelial progenitor cells. *Pharmaceutics* **2021**, *13*, 1152. DOI PubMed PMC
15. Bose, S.; Bhattacharjee, A.; Banerjee, D.; Boccaccini, A. R.; Bandyopadhyay, A. Influence of random and designed porosities on 3D printed tricalcium phosphate-bioactive glass scaffolds. *Addit. Manuf.* **2021**, *40*, 101895. DOI PubMed PMC
16. Jones, J. R. Review of bioactive glass: from hench to hybrids. *Acta. Biomater.* **2013**, *9*, 4457-86. DOI PubMed
17. Wang, G.; Lv, Z.; Wang, T.; et al. Surface functionalization of hydroxyapatite scaffolds with mgaleu-LDH nanosheets for high-performance bone regeneration. *Adv. Sci.* **2022**, *10*, e2204234. DOI

18. Vallet-Regi, M.; Salinas, A. J. Mesoporous bioactive glasses for regenerative medicine. *Mater. Today. Bio.* **2021**, *11*, 100121. DOI PubMed PMC
19. Sheng, X.; Li, C.; Wang, Z.; et al. Advanced applications of strontium-containing biomaterials in bone tissue engineering. *Mater. Today. Bio.* **2023**, *20*, 100636. DOI PubMed PMC
20. Li, Y.; Chen, L.; Chen, X.; et al. High phosphate content in bioactive glasses promotes osteogenesis *in vitro* and *in vivo*. *Dent. Mater.* **2021**, *37*, 272-83. DOI
21. Dai, Q.; Li, Q.; Gao, H.; et al. 3D printing of Cu-doped bioactive glass composite scaffolds promotes bone regeneration through activating the HIF-1α and TNF-α pathway of hUVECs. *Biomater. Sci.* **2021**, *9*, 5519-32. DOI
22. Signorelli, G. C.; Bianchetti, M. G.; Jermini, L. M. M.; et al. Dietary chloride deficiency syndrome: pathophysiology, history, and systematic literature review. *Nutrients* **2020**, *12*, 3436. DOI PubMed PMC
23. Chen, X.; Karpukhina, N.; Brauer, D. S.; Hill, R. G. Novel highly degradable chloride containing bioactive glasses. *Biomedical. Glasses.* **2015**, 1. DOI
24. Chen, X.; Chen, X.; Pedone, A.; Apperley, D.; Hill, R. G.; Karpukhina, N. New insight into mixing fluoride and chloride in bioactive silicate glasses. *Sci. Rep.* **2018**, *8*, 1316. DOI PubMed PMC
25. Chen, X.; Liu, Y.; Zhao, Y.; et al. Halide-containing bioactive glasses enhance osteogenesis *in vitro* and *in vivo*. *Biomater. Adv.* **2022**, *143*, 213173. DOI
26. Cortez, P. P.; Brito, A. F.; Kapoor, S.; et al. The *in vivo* performance of an alkali-free bioactive glass for bone grafting, FastOs® BG, assessed with an ovine model. *J Biomed Mater Res B Appl Biomater* 2017;105:30-8.[DOI:10.1002/jbm.b.33529] Caution!
27. Tajvar, S.; Hadjizadeh, A.; Samandari, S. S. Scaffold degradation in bone tissue engineering: an overview. *Int. Biodeterior. Biodegrad.* **2023**, *180*, 105599. DOI
28. Lee, I.; Shin, S.; Foroutan, F.; Lakhkar, N. J.; Gong, M.; Knowles, J. C. Effects of magnesium content on the physical, chemical and degradation properties in a MgO-CaO-Na_2O-P_2O_5 glass system. *J. Non-Cryst. Solids.* **2013**, *363*, 57-63. DOI
29. Wetzel, R.; Bartzok, O.; Brauer, D. S. Influence of low amounts of zinc or magnesium substitution on ion release and apatite formation of bioglass 45S5. *J. Mater. Sci. Mater. Med.* **2020**, *31*, 86. DOI PubMed PMC
30. Alawi AM, Majoni SW, Falhammar H. Magnesium and human health: perspectives and research directions. *Int. J. Endocrinol.* **2018**, *2018*, 9041694. DOI PubMed PMC
31. Nielsen, F. H. Magnesium deficiency and increased inflammation: current perspectives. *J. Inflamm. Res.* **2018**, *11*, 25-34. DOI PubMed PMC
32. Hohenbild, F.; Arango, O. M.; Schmitz, S. I.; Moghaddam, A.; Boccaccini, A. R.; Westhauser, F. An *in vitro* evaluation of the biological and osteogenic properties of magnesium-doped bioactive glasses for application in bone tissue engineering. *Int. J. Mol. Sci.* **2021**, *22*, 12703. DOI PubMed PMC
33. Dai, Q.; Wang, Z.; Liu, C.; Chen, X.; Cao, X. High performance injectable Mg doped bioactive glass bone cement for the regulation of osteogenic immune microenvironment. *Biomater. Adv.* **2024**, *160*, 213864. DOI
34. Chen, X.; Wang, M.; Kenny, C.; Chen, X.; Karpukhina, N.; Hill, R. G. Novel fluoride- and chloride-containing bioactive glasses for use in air abrasion. *J. Dent.* **2022**, *125*, 104252. DOI
35. Zeng, Y.; Deng, J. J.; Jiang, Q. L.; et al. Thyrotropin inhibits osteogenic differentiation of human periodontal ligament stem cells. *J. Periodontal. Res.* **2023**, *58*, 668-78. DOI
36. Han, Y.; Liu, C.; Chen, B.; et al. Orchestrated tumor apoptosis (Cu^{2+}) and bone tissue calcification (Ca^{2+}) by hierarchical copper/calcium-ensembled bioactive silica for osteosarcoma therapy. *Chem. Eng. J.* **2022**, *435*, 134820. DOI
37. Chen, X.; Chen, X.; Brauer, D. S.; et al. Sodium is not essential for high bioactivity of glasses. *Int. J. Appl. Glass. Sci.* **2017**, *8*, 428-37. DOI PubMed PMC
38. Kim, J.; Gilbert, J. L. The effect of cell density, proximity, and time on the cytotoxicity of magnesium and galvanically coupled magnesium-titanium particles *in vitro*. *J. Biomed. Mater. Res. A.* **2018**, *106*, 1428-39. DOI PubMed
39. Martin, D.; Cooper, S. B.; Tang, J. C. Y.; Fraser, W. D.; Sale, C.; Elliott-Sale, K. J. Bone metabolic marker concentrations across the menstrual cycle and phases of combined oral contraceptive use. *Bone* **2021**, *145*, 115864. DOI PubMed
40. Zhong, Y.; Liu, C.; Yan, X.; Li, X.; Chen, X.; Mai, S. Odontogenic and anti-inflammatory effects of magnesium-doped bioactive glass in vital pulp therapy. *Biomed. Mater.* **2024**, 19. DOI
41. Lin, S.; Cao, L.; Wang, Q.; et al. Tailored biomimetic hydrogel based on a photopolymerised DMP1/MCF/gelatin hybrid system for calvarial bone regeneration. *J. Mater. Chem. B.* **2018**, *6*, 414-27. DOI
42. Chu, W.; Li, T.; Jia, G.; et al. Exposure to high levels of magnesium disrupts bone mineralization *in vitro* and *in vivo*. *Ann. Transl. Med.* **2020**, *8*, 1419. DOI PubMed PMC
43. Khotib, J.; Marhaeny, H. D.; Miatmoko, A.; et al. Differentiation of osteoblasts: the links between essential transcription factors. *J. Biomol. Struct. Dyn.* **2023**, *41*, 10257-76. DOI
44. Gomathi, K.; Akshaya, N.; Srinaath, N.; Moorthi, A.; Selvamurugan, N. Regulation of Runx2 by post-translational modifications in osteoblast differentiation. *Life. Sci.* **2020**, *245*, 117389. DOI PubMed
45. Burger, M. G.; Grosso, A.; Briquez, P. S.; et al. Robust coupling of angiogenesis and osteogenesis by VEGF-decorated matrices for bone regeneration. *Acta. Biomater.* **2022**, *149*, 111-25. DOI
46. Li, X.; Wang, M.; Zhang, W.; et al. A magnesium-incorporated nanoporous titanium coating for rapid osseointegration. *Int. J. Nanomedicine.* **2020**, *15*, 6593-603. DOI

47. Wang, J.; Yang, B.; Guo, S.; Yu, S.; Li, H. Manufacture of titanium alloy materials with bioactive sandblasted surfaces and evaluation of osseointegration properties. *Front. Bioeng. Biotechnol.* **2023**, *11*, 1251947. DOI PubMed PMC
48. Cheng, C.; Chaaban, M.; Born, G.; et al. Repair of a rat mandibular bone defect by hypertrophic cartilage grafts engineered from human fractionated adipose tissue. *Front. Bioeng. Biotechnol.* **2022**, *10*, 841690. DOI PubMed PMC
49. Zhao, D.; Wang, X.; Cheng, B.; et al. Degradation-kinetics-controllable and tissue-regeneration-matchable photocross-linked alginate hydrogels for bone repair. *ACS. Appl. Mater. Interfaces.* **2022**, *14*, 21886-905. DOI
50. Lioubavina-Hack, N.; Carmagnola, D.; Lynch, S. E.; Karring, T. Effect of Bio-Oss® with or without platelet-derived growth factor on bone formation by "guided tissue regeneration": a pilot study in rats. *J. Clin. Periodontol.* **2005**, *32*, 1254-60. DOI PubMed
51. Jithendra, P.; Mohamed, J. M. M.; Annamalai, D.; et al. Biopolymer collagen-chitosan scaffold containing aloe vera for chondrogenic efficacy on cartilage tissue engineering. *Int. J. Biol. Macromol.* **2023**, *248*, 125948. DOI
52. Ge, R.; Xun, C.; Yang, J.; Jia, W.; Li, Y. *In vivo* therapeutic effect of wollastonite and hydroxyapatite on bone defect. *Biomed. Mater.* **2019**, *14*, 065013. DOI
53. Wang, L.; Wan, L.; Zhang, T.; et al. A combined treatment of BMP2 and soluble VEGFR1 for the enhancement of tendon-bone healing by regulating injury-activated skeletal stem cell lineage. *Am. J. Sports. Med.* **2024**, *52*, 779-90. DOI
54. Sahin, E.; Orhan, C.; Balci, T. A.; Erten, F.; Sahin, K. Magnesium picolinate improves bone formation by regulation of RANK/RANKL/OPG and BMP-2/Runx2 signaling pathways in high-fat fed Rats. *Nutrients* **2021**, *13*, 3353. DOI PubMed PMC
55. Zhang, J.; Tang, L.; Qi, H.; Zhao, Q.; Liu, Y.; Zhang, Y. Dual function of magnesium in bone biomineralization. *Adv. Healthc. Mater.* **2019**, *8*, e1901030. DOI
56. Sun, Y.; Helmholz, H.; Willumeit-römer, R. Systemic modulation of skeletal mineralization by magnesium implant promoting fracture healing: radiological exploration enhanced with PCA-based machine learning in a rat femoral model. *J. Magnes. Alloys.* **2024**, *12*, 1009-20. DOI
57. Sayed, A. S.; El-Saadany, H. M.; Kotb, G. A. M.; et al. Biosafety evaluation of two beauveria bassiana products on female albino rats using acute oral test. *Saudi. J. Biol. Sci.* **2022**, *29*, 103293. DOI PubMed PMC
58. Tan, G.; Chen, R.; Tu, X.; et al. Research on the osteogenesis and biosafety of ECM-loaded 3D-printed Gel/SA/58sBG scaffolds. *Front. Bioeng. Biotechnol.* **2022**, *10*, 973886. DOI
59. Yang, Z.; Liu, X.; Zhao, F.; et al. Bioactive glass nanoparticles inhibit osteoclast differentiation and osteoporotic bone loss by activating lncRNA NRON expression in the extracellular vesicles derived from bone marrow mesenchymal stem cells. *Biomaterials* **2022**, *283*, 121438. DOI
60. Hu, S.; Wang, S.; He, Q.; et al. A mechanically reinforced super bone glue makes a leap in hard tissue strong adhesion and augmented bone regeneration. *Adv. Sci.* **2023**, *10*, e2206450. DOI